Available online at www.sciencedirect.com
ScienceDirect
Journal of Sound and Vibration 311 (2008) 652–666
JOURNAL OF SOUND AND VIBRATION
www.elsevier.com/locate/jsvi

Control of multi-dof ultrasonic actuator for dexterous surgical instrument

Kenjiro Takemura[a], Shinsuk Park[b,*], Takashi Maeno[c]

[a]*Precision and Intelligence Laboratory, Tokyo Institute of Technology, 4925 Nagatsuta-cho, Midori-ku, Yokohama 226-8523, Japan*
[b]*Department of Mechanical Engineering, Korea University, Anam-dong, Sungbuk-gu, Seoul 136-713, Republic of Korea*
[c]*Department of Mechanical Engineering, Keio University, 3-14-1 Hiyoshi, Kohoku-ku, Yokohama 223-8522, Japan*

Received 6 March 2006; received in revised form 19 August 2007; accepted 23 September 2007
Available online 26 November 2007

Abstract

For surgical devices used in minimally invasive surgery, compact multi-degree-of-freedom (multi-dof) actuators are required due to a small work space in the patient body. With conventional single-dof actuators such as electromagnetic motors, a multiple number of actuators are required to generate multi-dof motion. Moreover, additional transmission mechanisms make the total system even larger and heavier. In contrast, a single unit of multi-dof ultrasonic actuator can generate multi-dof rotation of a spherical rotor by utilizing three natural vibration modes of a bar-shaped stator. In our previous work we designed and built a surgical forceps with a wrist capable of two-dof motion, using a single multi-dof ultrasonic motor. The present study proposes a novel control scheme to generate three-dof motion of the surgical instrument for minimally invasive surgical procedures. Through experiments we have confirmed the system performance of the developed device.

1. Introduction

For the past decade robots have been appearing in the field of medical applications. Those robots improve precision, repeatability, stability, and dexterity, and commercialized surgical robots are now being used in minimally invasive surgery (MIS) [1]. MIS is performed using long tools inserted into the patient's body through small incisions, where the surgeon manipulates the tools from outside the patient's body. Visual feedback is available using an endoscope, which is also inserted into the body and transmits video images of the surgical site to a video monitor. This surgical method offers many advantages including reduced patient pain and trauma, fewer complications, and shorter recovery periods. In MIS, however, small and dexterous surgical devices are required, for the surgeon to work through small incisions that are much smaller than would be required to perform an open surgery.

For surgical manipulations in the patient body, actuators capable of generating a sufficient number of degrees of freedom (dof) are desirable. With general electromagnetic motors, the number of motors should be

*Corresponding author. Tel.: +82 2 3290 3373; fax: +82 2 926 9290.
E-mail addresses: takemura@pi.titech.ac.jp (K. Takemura), drsspark@korea.ac.kr (S. Park), maeno@mech.keio.ac.jp (T. Maeno).

0022-460X/$ - see front matter © 2007 Elsevier Ltd. All rights reserved.
doi:10.1016/j.jsv.2007.09.040

equal to or larger than the number of dof, since the electromagnetic motors can only generate single-dof rotational motion. Moreover, transmission mechanisms to obtain larger torque make the total system larger and heavier. In contrast, ultrasonic motors have characteristics including high torque capacity at low speed, high stationary limiting torque, low electromagnetic radiation, and simplicity of design. There have been a number of studies on multi-dof actuators, utilizing the principle of ultrasonic motors. Bansevicius [2] developed a piezoelectric multi-dof actuator that consists of a cylindrical stator (vibrator) and a spherical rotor. In a multi-dof ultrasonic actuator developed by Amano et al. [3] a spherical rotor rotates along three perpendicular axes. Toyama [4] devised an ultrasonic motor consisting of three ring-shaped stators and a spherical rotor. Sasae et al. [5] constructed a three-dof actuation unit composed of a spherical rotor and a truss structure of piezoelectric ceramics.

Though ultrasonic motors are well suited to multi-dof actuation, they are not yet competent enough to replace general electromagnetic motors, owing to their limited output torque, low controllability and difficulty in fabricating the design. To enhance the performance of multi-dof ultrasonic motors, more precise geometric design of the stator and sophisticated motion control scheme are required.

Our previous study developed an ultrasonic motor capable of multi-dof actuation [6,7]. The developed ultrasonic motor generates a multi-dof rotation of a spherical rotor using three natural vibration modes of a bar-shaped stator. In our other study, we designed and built a multi-dof surgical instrument with a wrist, where *two*-dof rotation (pitch and yaw) is actuated by the ultrasonic motor under joystick control [8].

The present study proposes a novel control scheme to control *three*-dof motion of the surgical instrument system that is designed under the concept of master–slave system control. The control scheme allows us to control full three-dof motion (spin, pitch and yaw) of the wrist by introducing one more dof (spin) to the system, which is useful in many surgical procedures. The performance of the system has been evaluated through experiments.

2. Multi-dof ultrasonic actuator

An ultrasonic motor is composed of a stator (vibrator) and a rotor. The vibrational energy of the stator is transmitted to the rotor by the frictional force between the stator and the rotor. Single-dof ultrasonic motors utilize two natural vibration modes of the stator to generate a single-dof rotation of the rotor. By exciting the two vibration modes, points on the stator surface draw oval trajectories, and those trajectories, in turn, frictionally drive the rotor along a specific axis, when the rotor is in contact with the stator. Our previous study extended this idea to the generation of multi-dof motion by exciting three vibration modes of the stator and coordinating the directions of the three modes to be perpendicular to each other [6,7]. The multi-dof ultrasonic motor we developed consists of a bar-shaped stator and a spherical rotor as shown in Fig. 1. The spherical rotor can be rotated around three perpendicular axes by combining the first longitudinal vibration mode and two second bending vibration modes of the stator (Fig. 2). Findings from our previous study suggest the following design requirements for the stator:

(i) Natural frequencies of three vibration modes are nearly the same.
(ii) Natural frequencies of three vibration modes are low enough to avoid the excitement of higher vibration modes.
(iii) Motions of three vibration modes are perpendicular to each other.

Fig. 3 illustrates the driving principle of the multi-dof ultrasonic motor. In Fig. 3(a) the spherical rotor is rotated around z-axis by combining the bending modes in zx-plane and yz-plane denoted as (i) (iii) and (ii) (iv), respectively. When the two bending modes are excited at a phase difference of 90°, the rotor in contact with the stator head rotates along z-axis by frictional force applied by the stator. In Fig. 3(b) the spherical rotor is rotated around x-axis by combining the bending mode in yz-plane and the longitudinal mode along z-axis denoted as (i) (iii) and (ii) (iv), respectively. When the longitudinal mode and the bending mode are excited at a phase difference of 90°, the stator frictionally drives the rotor along x-axis. The same principle applies when the rotor is driven around y-axis; the longitudinal modes along z-axis and the bending mode in zx-plane are combined in the same way as in Fig. 3(b).

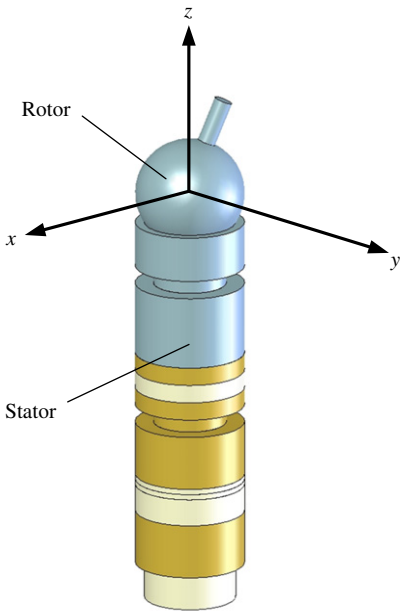

Fig. 1. Multi-dof ultrasonic motor.

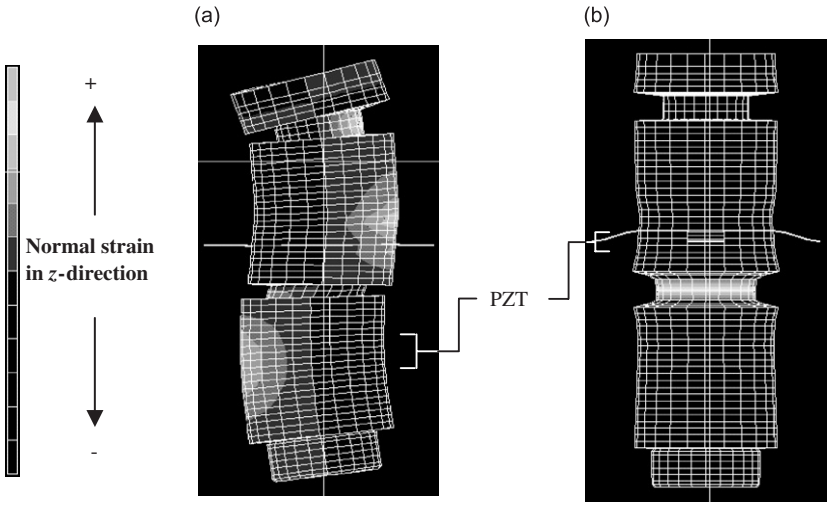

Fig. 2. Natural vibration modes of stator.

The geometry of the bar-shaped stator was designed using finite element analysis (Fig. 2), so that the natural frequencies of the longitudinal mode and the two bending modes correspond to each. As shown in Fig. 4, the stator consists of a head, rings, stacked piezoelectric rings and a shaft. The stator head, the rings, and the shaft are made of nickel-plated brass, brass, and stainless steel, respectively. The shaft is screwed up into the head as in Langevin type vibrator. The piezoelectric ceramic rings excite one longitudinal mode and two bending modes of the bar-shaped stator. The diameter and height of the stator are 10 and 30.8 mm, respectively. The rotor has a spherical shape and is made of stainless steel. The preload between the stator and rotor is provided by a magnetic disk. The natural frequencies of the three vibration modes were measured to be around 40 kHz. The torque capacity of the ultrasonic motor is dependent on the direction of rotation and the preload given between the rotor and the stator [9]. The maximum torque in a certain rotational direction can be expressed in a vector form, where the magnitude and the direction of the vector represent the maximum torque and the

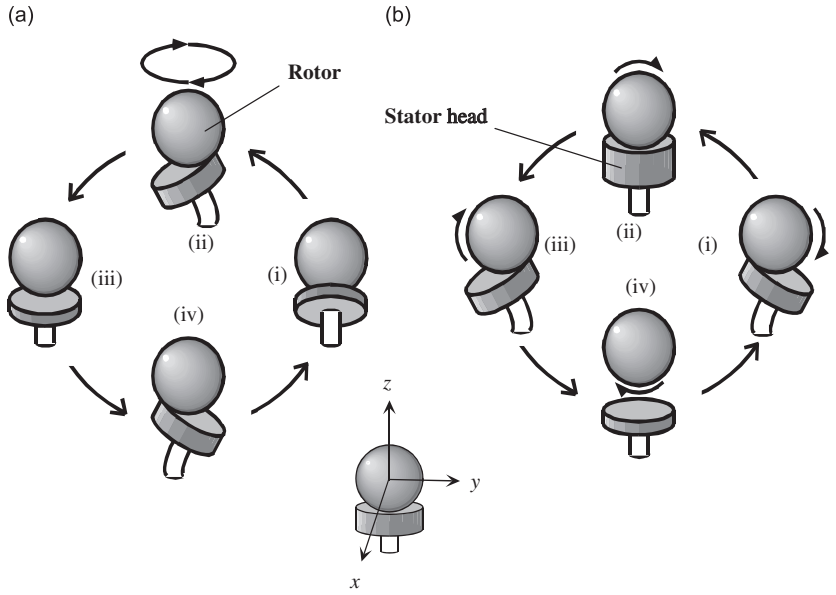

Fig. 3. Driving principle of multi-dof ultrasonic motor.

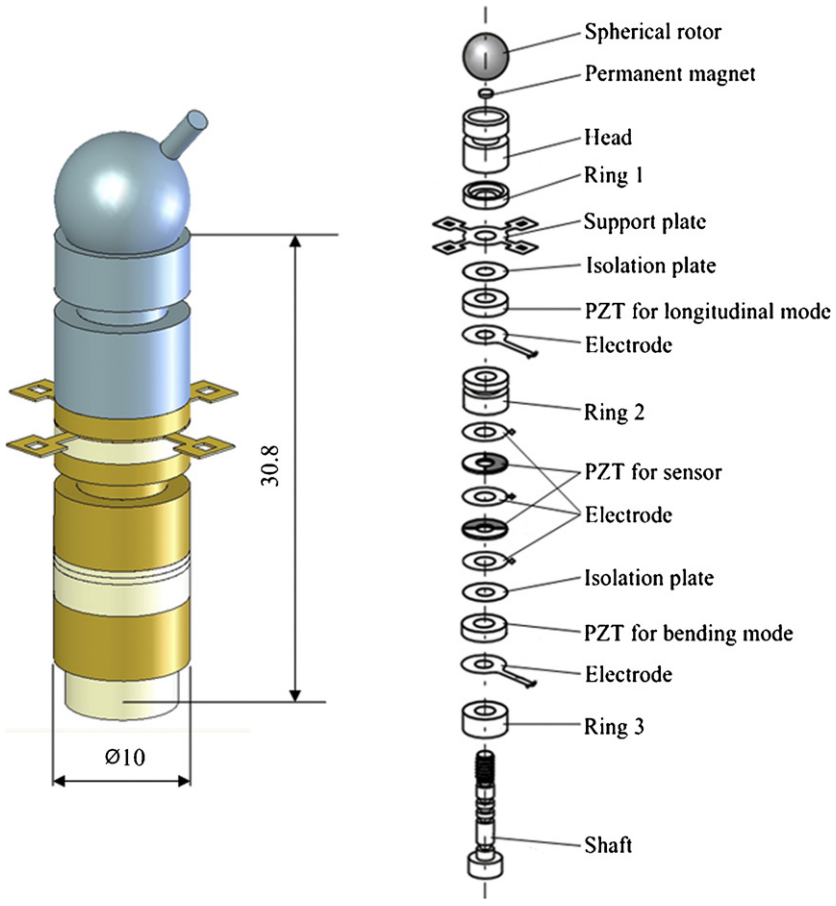

Fig. 4. Structure of multi-dof ultrasonic motor.

direction of rotation, respectively. Fig. 5 shows the surface of the maximum torque in the first octan with the preload of 4 N. By increasing the preload, the torque capacity can be improved. The maximum torque of 0.007 Nm was achieved with the preload of 6 N when the rotation is along z-axis.

The three vibration modes of the bar-shaped stator are driven by three sinusoidal input signals to piezoelectric actuators in the stator:

$$\begin{aligned} V_z &= A_z \sin(2\pi f_z + \phi_z), \\ V_x &= A_x \sin(2\pi f_x + \phi_x), \\ V_y &= A_y \sin(2\pi f_y + \phi_y), \end{aligned} \tag{1}$$

where V_z is the input signal for longitudinal vibration in z-direction, V_x the input signals for bending vibrations in zx-plane, V_y the input signals for bending vibrations in yz-plane, A_z the amplitude of input signal for longitudinal vibration in z-direction, A_x the amplitude of input signals for bending vibrations in zx-plane, A_y the amplitude of input signals for bending vibrations in yz-plane, f_z the frequency of input signal for longitudinal vibration in z-direction, f_x the frequencies of input signals for bending vibrations in zx-plane, f_y the frequencies of input signals for bending vibrations in yz-plane, φ_z the phase shift of input signal for longitudinal vibration in z-direction, φ_x the phase shifts of input signals for bending vibrations in zx-plane, and φ_y the phase shifts of input signals for bending vibrations in yz-plane.

To drive the rotor about an arbitrary axis, the frequencies, amplitudes and phase shifts of the input signals are chosen as operating parameters, which adds up to the total number of nine (A_x, A_y, A_z, f_x, f_y, f_z, φ_x, φ_y, and φ_z).

Fig. 6 shows the schematic view of USM driver circuit. Three square wave signals are generated using a function generator and a phase shifter. To acquire sinusoidal signals, the square waves pass through a low-pass filter with a cutoff frequency. The filtered signals are amplified and then drive the piezoelectric actuators of the stator.

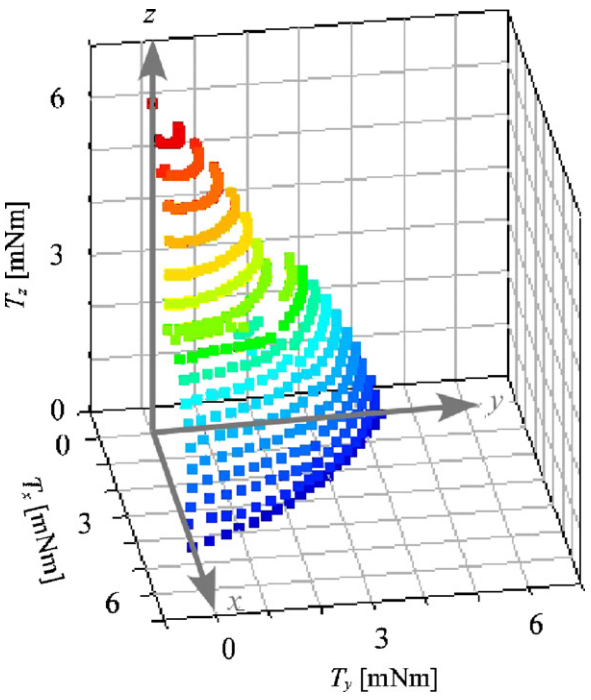

Fig. 5. Plot of maximum torque along rotational directions.

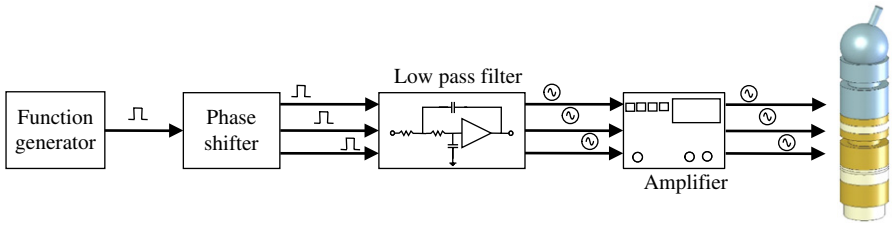

Fig. 6. Multi-dof USM driver circuit.

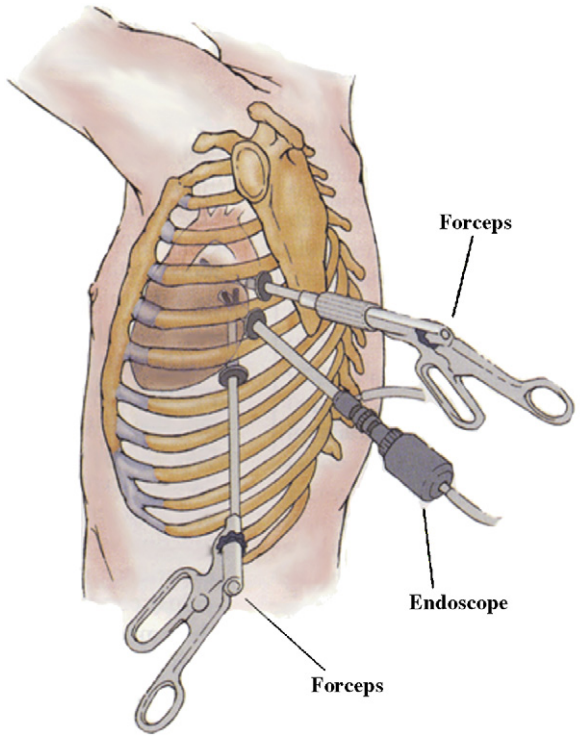

Fig. 7. Minimally invasive surgery.

3. Surgical instrument with ultrasonic actuator

During minimally invasive surgical procedures, surgical instruments and an endoscope are inserted through small incisions in the patient body (Fig. 7). The incision ports provide pivot points that allow three-dof rotational motion and single-dof translational motion (in-and-out motion) of the surgical instruments and the endoscope. Conventional surgical forcipes shown in the figure are straight and do not provide additional dof to the four dofs at incision ports. In minimally invasive procedures, surgeons experience many difficulties, including the issues of decreased visual and haptic information, motion constraints, and cognitive spatio-motor remapping, which is inherent to laparoscopic surgery [1]. Teleoperated surgical robots have been introduced to alleviate some of these issues by increasing dexterity and information available to the surgeon while maintaining the advantages of MIS.

With the ultrasonic actuator described above and teleoperation concept, our previous work developed a surgical instrument with a multi-dof wrist as shown in Fig. 8(a) [8]. The instrument consists of a wrist joint with an ultrasonic actuator, a gripper, potentiometers, and a joystick controller. Two-dof rotational motion (pitch and yaw) of the gripper was controlled by the joystick controller, under master–slave system control scheme.

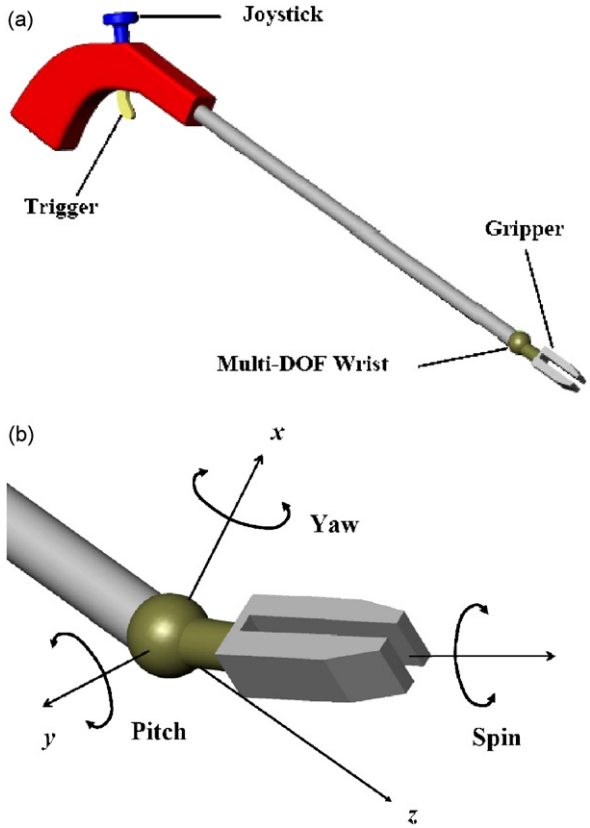

Fig. 8. Design of multi-dof surgical instrument.

In the present study, a novel control scheme is introduced to control three-dof rotational motion, by enabling spin motion at the wrist. The actuated wrist joint controls pitch, yaw and spin motions of the forceps, where pitch motion is the rotation along y-axis, yaw motion along x-axis, and spin motion along the centerline of gripper (Fig. 8(b)). In addition to the four-dof global motion at the pivot point, implementing three extra dof (spin, pitch and yaw) in the wrist enables more precise and dexterous surgical operations: pitch and yaw motions are useful in accessing the surgical site, and spin motion enables suturing and knotting procedures.

Fig. 9(a) shows a master–slave system we have constructed based on the design described above. A thumb-controlled joystick serves as the master port (Fig. 9(b)), and the forceps with the actuated wrist constitutes the slave port (Fig. 9(c)).

Fig. 10 illustrates the schematic view of master–slave system control. The controller of the system is implemented on a PC. The pitch and yaw angles of the master and the slave are measured by two potentiometers equipped on the joystick and by two potentiometers equipped on the wrist with the ultrasonic motor, respectively. The angle data from the potentiometers of the joystick and the wrist is sent to the PC through A/D converter. Based on the driving principle of the multi-dof ultrasonic motor, three sinusoidal input signals to the multi-dof ultrasonic motor are generated using the USM driver circuit. Both the function generator and the phase shifter of the USM driver circuit are implemented on Field Programmable Gate Array (FPGA). The controller program for the master–slave system was developed on Turbo C++ in MS-DOS environment. Real-time control at 500 Hz was used for the master–slave system control.

Different control schemes are employed to control the pitch–yaw motion and the spin motion. Pitch and yaw *angles* are controlled through feedback control, which requires angle measurements. The spin *speed* is controlled in open-loop manner without needing to measure the spin angle or speed. While the spin motion of

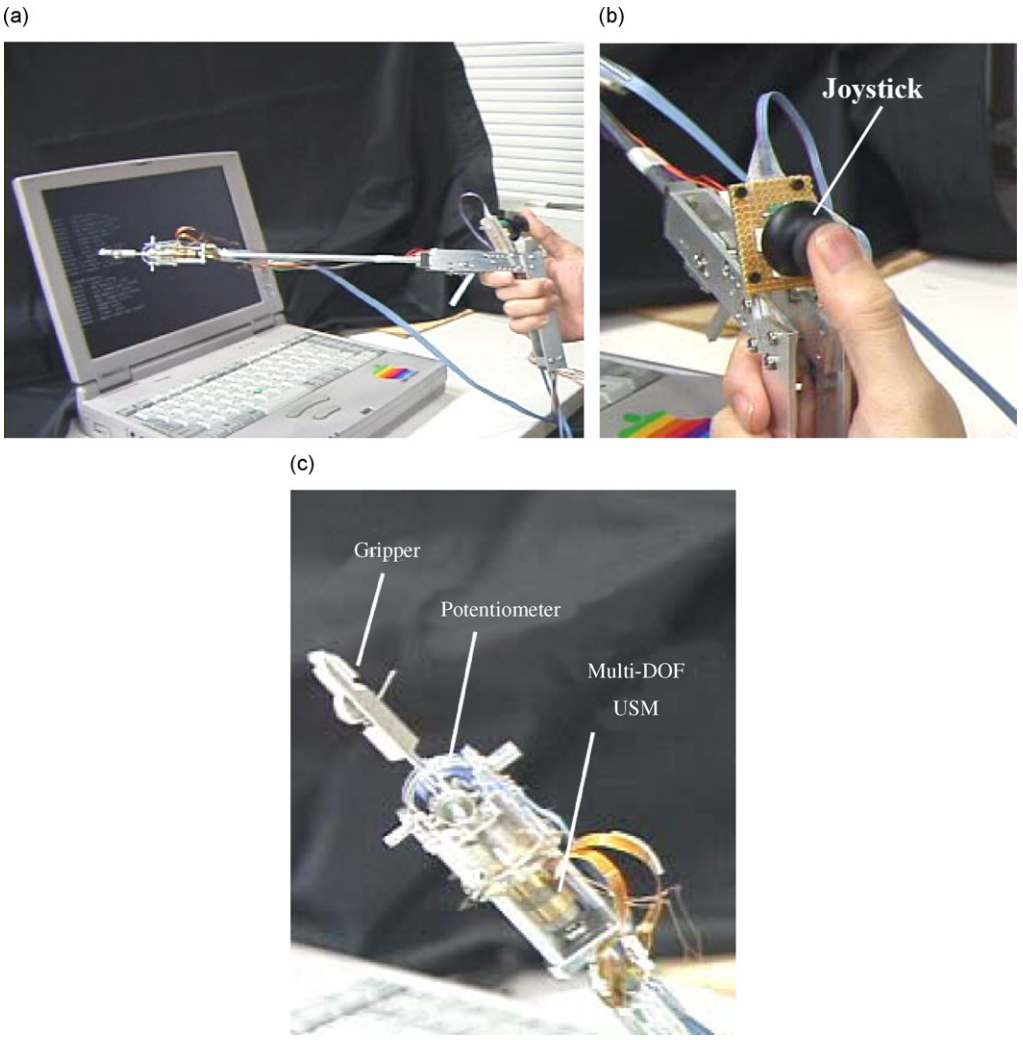

Fig. 9. Master–slave system for surgical instrument.

the instrument is useful for suturing and knotting, those procedures can be performed with a constant rotational speed. The instrument was designed to have a fixed rotational speed for spin motion, while the direction of spin, clockwise or counterclockwise, can be switched.

While the angular position of the wrist can be controlled by modulating the nine operating parameters of the three sinusoidal signals, four parameters and six parameters were chosen to control pitch–yaw motion and spin motion, respectively.

3.1. Control of pitch–yaw motion of wrist

Our previous study developed a simple control scheme for pitch–yaw motion control [8]. In controlling the pitch and yaw motions, two amplitudes (A_x and A_y) and two phase shifts (φ_x and φ_y) of the two bending vibration modes are modulated to control the angular position of the wrist along x-direction (yaw) and along y-direction (pitch): amplitudes A_x and A_y are controlled using a proportional controller, and phase shifts φ_x and φ_y are modulated at discrete values. The frequencies (f_z, f_x, and f_y) of three sinusoidal signals are kept at 40 kHz, and the amplitude and phase shift (A_z and φ_z) for the longitudinal vibration mode are kept constant (Table 1).

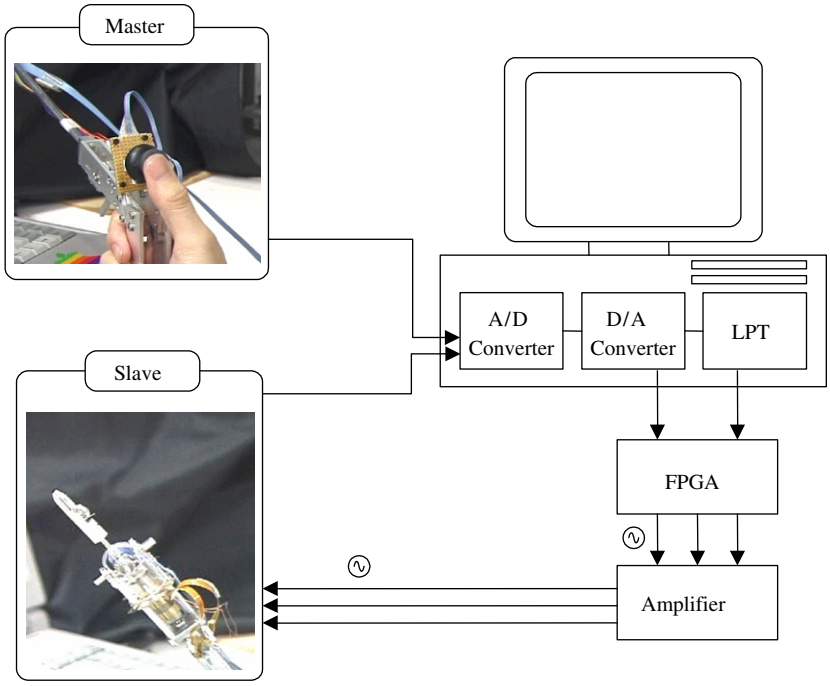

Fig. 10. Control of master–slave system.

Table 1
Control of pitch–yaw motion

	Longitudinal vibration (z-axis)	Bending vibration (zx-plane)	Bending vibration (yz-plane)
Amplitude	$A_z = 20$ [V] = const	$A_x = K_p\lvert\theta_{\text{pitch}} - \theta^d_{\text{pitch}}\rvert + \varepsilon$	$A_x = K_p\lvert\theta_{\text{yaw}} - \theta^d_{\text{yaw}}\rvert + \varepsilon$
Phase shift	$\varphi_z = \pi/2 = \text{const}$	$\varphi_x = 0(\theta_{\text{pitch}} - \theta^d_{\text{pitch}} < 0)$	$\varphi_y = 0(\theta_{\text{yaw}} - \theta^d_{\text{yaw}} < 0)$
		$= \pi(\theta_{\text{pitch}} - \theta^d_{\text{pitch}} > 0)$	$= \pi(\theta_{\text{yaw}} - \theta^d_{\text{yaw}} > 0)$
Frequency	$f_z = 40\,\text{kHz} = \text{const}$	$f_x = 40\,\text{kHz} = \text{const}$	$f_y = 40\,\text{kHz} = \text{const}$

K_p = proportional gain, θ_{yaw}, θ_{pitch} = yaw and pitch angles of slave, θ^d_{yaw}, θ^d_{pitch} = yaw and pitch angles of master, ε = bias.

3.2. Control of spin motion of wrist

While the pitch and yaw motions are controlled by a rather simple control scheme, a more sophisticated strategy is employed in controlling the spin motion of the wrist. Considering the driving principle of the multi-dof ultrasonic motor, six independent parameters out of the nine operating parameters are chosen to control the spin motion: three amplitudes (A_x, A_y, and A_z) and three phase shifts (φ_x, φ_y, and φ_z) of three vibration modes (one longitudinal mode and two bending modes) are modulated, while the frequencies (f_x, f_y, and f_z) of the three sinusoidal signals are kept at 40 kHz, as in pitch–yaw motion control.

For a given spin motion, the corresponding values for the six parameters cannot be determined uniquely. Our previous study developed an inverse model which maps from spin velocity (the direction and the rotational speed) to the six operating parameters of the multi-dof ultrasonic motor [7]. The spin velocity can be represented by spin vector $\mathbf{S}$ (S_x, S_y, S_z), and spin vector $\mathbf{S}$ can be classified into 24 categories depending on where the direction of spin vector $\mathbf{S}$ lies (Table 2). As can be seen in the look-up table of driving states, four parameters out of the six parameters are determined, and two operating parameters (A and φ) still remain to be determined. The relationship between the remaining two parameters and spin vector $\mathbf{S}$ is nonlinear. To deal

Table 2
Look-up table for control of spin motion

Category	Quadrant where spin vector **S** lies	Maximum component of spin vector **S**	Phase shifts			Ratio of amplitudes
			φ_x	φ_y	φ_z	$A_x : A_y : A_z$
1		S_x ($\|S_x\| > \|S_y\|, \|S_z\|$)	φ	$\pi/2$	0	**A** : 1 : 1
2	(+, +, −)	S_y ($\|S_y\| > \|S_z\|, \|S_x\|$)	0	φ	$\pi/2$	1 : **A** : 1
3		S_z ($\|S_z\| > \|S_x\|, \|S_y\|$)	0	$\pi/2$	φ	1 : 1 : **A**
4		S_x ($\|S_x\| > \|S_y\|, \|S_z\|$)	φ	$\pi/2$	0	**A** : 1 : 1
5	(+, −, +)	S_y ($\|S_y\| > \|S_z\|, \|S_x\|$)	$\pi/2$	φ	0	1 : **A** : 1
6		S_z ($\|S_z\| > \|S_x\|, \|S_y\|$)	$\pi/2$	0	φ	1 : 1 : **A**
7		S_x ($\|S_x\| > \|S_y\|, \|S_z\|$)	φ	$\pi/2$	0	**A** : 1 : 1
8	(+, −, −)	S_y ($\|S_y\| > \|S_z\|, \|S_x\|$)	$\pi/2$	φ	0	1 : **A** : 1
9		S_z ($\|S_z\| > \|S_x\|, \|S_y\|$)	0	$\pi/2$	φ	1 : 1 : **A**
10		S_x ($\|S_x\| > \|S_y\|, \|S_z\|$)	φ	0	$\pi/2$	**A** : 1 : 1
11	(−, +, +)	S_y ($\|S_y\| > \|S_z\|, \|S_x\|$)	0	φ	$\pi/2$	1 : **A** : 1
12		S_z ($\|S_z\| > \|S_x\|, \|S_y\|$)	$\pi/2$	0	φ	1 : 1 : **A**
13		S_x ($\|S_x\| > \|S_y\|, \|S_z\|$)	φ	0	$\pi/2$	**A** : 1 : 1
14	(−, +, −)	S_y ($\|S_y\| > \|S_z\|, \|S_x\|$)	0	φ	$\pi/2$	1 : **A** : 1
15		S_z ($\|S_z\| > \|S_x\|, \|S_y\|$)	0	$\pi/2$	φ	1 : 1 : **A**
16		S_x ($\|S_x\| > \|S_y\|, \|S_z\|$)	φ	0	$\pi/2$	**A** : 1 : 1
17	(−, −, +)	S_y ($\|S_y\| > \|S_z\|, \|S_x\|$)	$\pi/2$	φ	0	1 : **A** : 1
18		S_z ($\|S_z\| > \|S_x\|, \|S_y\|$)	$\pi/2$	0	φ	1 : 1 : **A**
19		S_x ($\|S_x\| > \|S_y\|, \|S_z\|$)	φ	$\pi/2$	0	**A** : 1 : 1
20	(+, +, +)	S_y ($\|S_y\| > \|S_z\|, \|S_x\|$)	0	φ	$\pi/2$	1 : **A** : 1
21		S_z ($\|S_z\| > \|S_x\|, \|S_y\|$)	$\pi/2$	0	φ	1 : 1 : **A**
22		S_x ($\|S_x\| > \|S_y\|, \|S_z\|$)	φ	$-\pi/2$	0	**A** : 1 : 1
23	(−, −, −)	S_y ($\|S_y\| > \|S_z\|, \|S_x\|$)	0	φ	$-\pi/2$	1 : **A** : 1
24		S_z ($\|S_z\| > \|S_x\|, \|S_y\|$)	$-\pi/2$	0	φ	1 : 1 : **A**

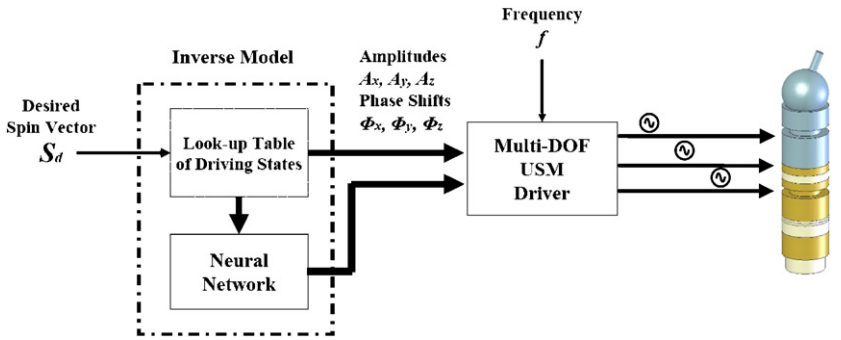

Fig. 11. Control of spin motion.

with the nonlinearity, three-layer neural networks are used to determine the remaining two parameters. Connective weights of the neural networks are trained according to the error back propagation algorithm using teacher signals [10]. The teacher signals to train the neural networks are obtained from the forward dynamics model of the multi-dof ultrasonic motor [11].

Fig. 11 illustrates the control scheme for the spin motion. After the direction of desired spin vector $\mathbf{S}_d$ is identified among the 24 categories, the inverse model determines four parameter (two amplitudes and two phase shifts) from Table 2 and, then, two remaining parameters (one amplitude and one phase shift) from neural networks. With the determined six operation parameters, the spin motion of the wrist can be controlled.

4. Experiments

The performance of the master–slave system of the surgical instrument is examined through experiments. For the pitch–yaw motion, the step response with the target position at 10° was measured as shown in Fig. 12(a). The figure shows undershoot upon the onset of the step input, and the rise time (0–100%) was estimated to be around 35 ms. Fig. 12(b) illustrates the plots of the pitch and yaw angles with an arbitrary

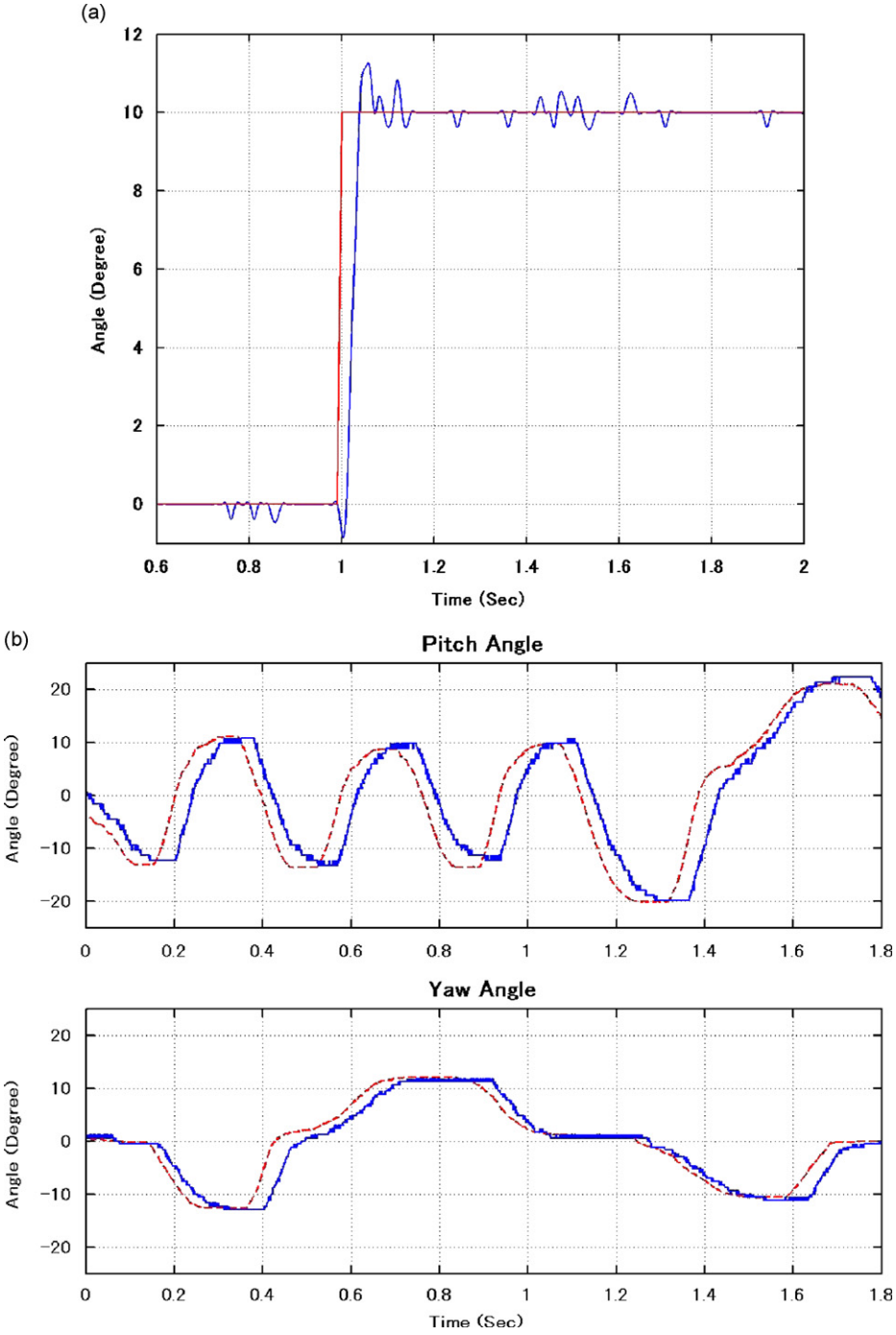

Fig. 12. Master–slave system performance.

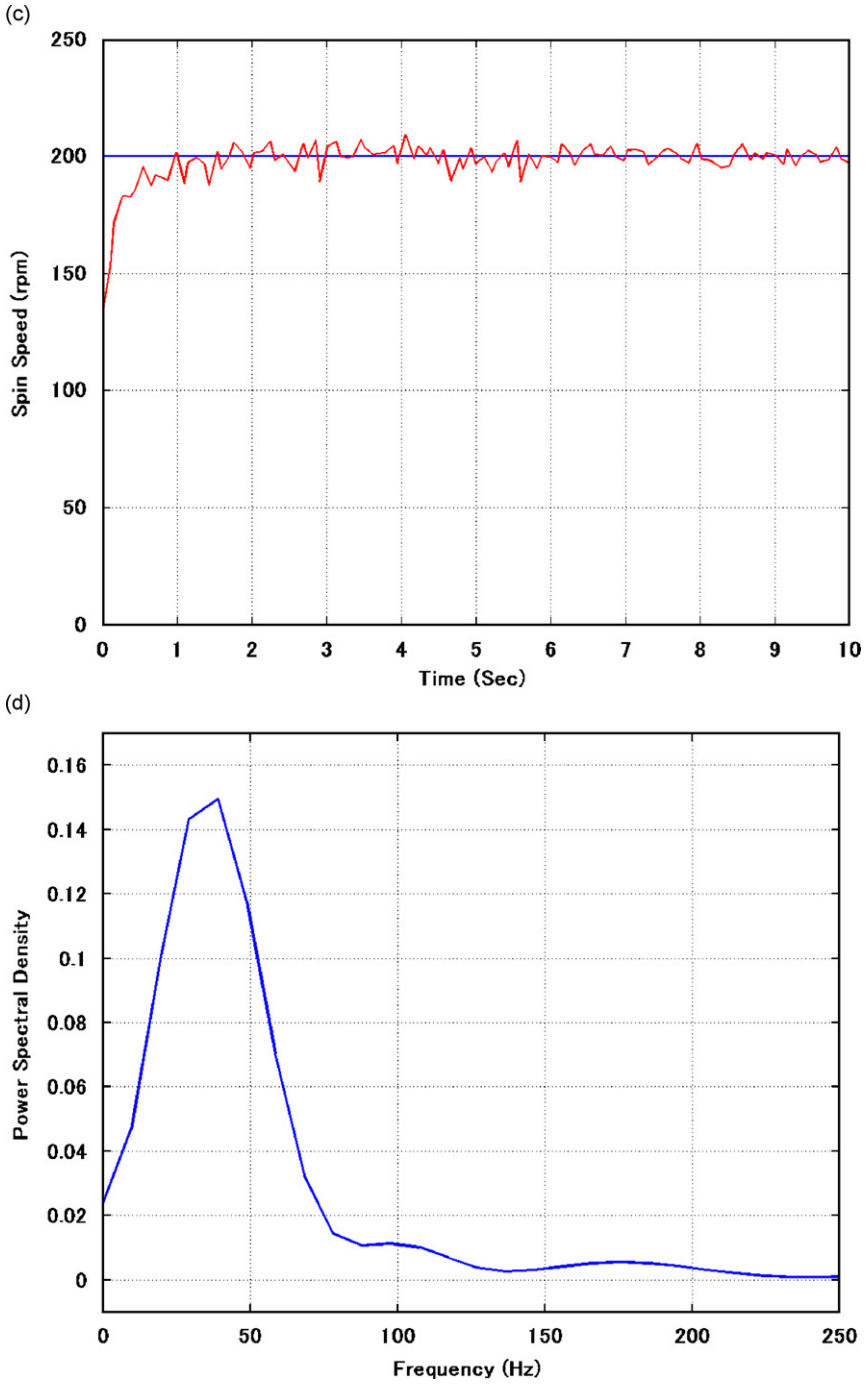

Fig. 12. (*Continued*)

master input by the thumb. As can be seen in the figure, there was a delay in the slave output in the order of tens of milliseconds. The response delays probably result from slippage between the stator and rotor surfaces. To quantify the time delay between the master and the slave, cross-correlation of the master input and the slave output were measured. With an impulsive master input, the time delay can be obtained from the location of peak point of cross-correlation function. The peak points of cross-correlation functions were typically around 70 ms, which can be interpreted that there was a time delay of approximately 70 ms in the slave output.

For the spin motion, the step response of the spin speed to the target speed of 200 rev/min was measured (Fig. 12(c)). While the pitch and yaw motions can be measured using the potentiometers at the wrist, the surgical instrument has no sensors to measure the spin motion. The spin speed was measured by aligning a rotary encoder with a determined spin axis. The spin speed appears to converge to the steady state with some oscillations around 200 rev/min.

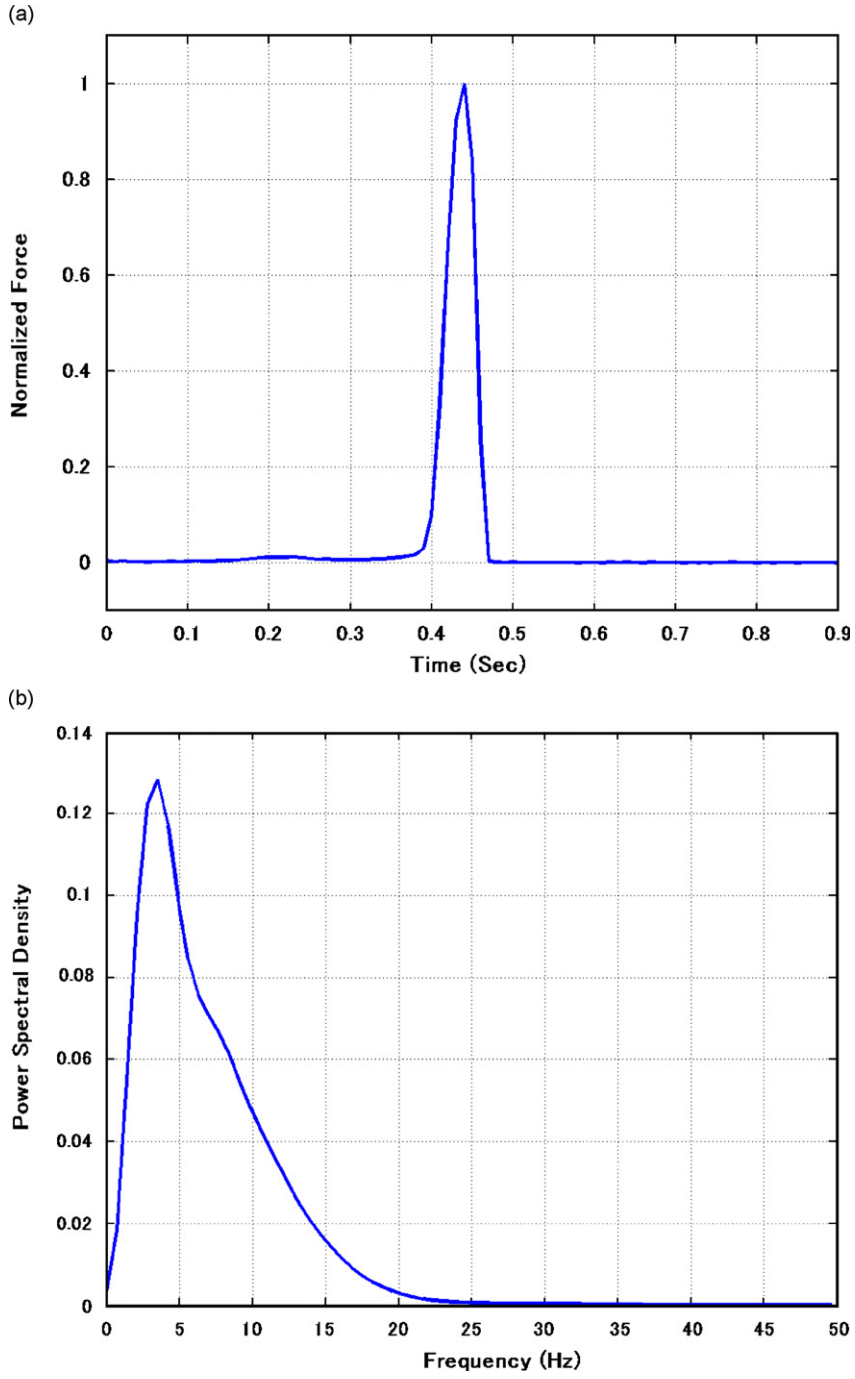

Fig. 13. Impulsive finger force and its power spectral density function.

The mechanical bandwidth of the master–slave system was estimated by measuring the slave output when a sharp impulse was given at the master port. Fig. 12(d) shows the power spectral density function of the slave response. 50% energy bandwidth, the frequency band in which 50% of its power is located, was used as an estimation of the speed of system response. The bandwidth for the master–slave system was estimated to be around 48 Hz.

To compare with the master–slave system bandwidth, the bandwidth of the human finger movement was estimated. To measure the finger force, seven human subjects were asked to apply a sharp jerky force by the thumb on a force transducer (JR3 67M25A) as quickly as they can. The subjects were all male students of Korea University, ranged in age from 21 to 27. By assuming that an impulsive force includes the highest frequency components of the finger movement, the power spectral density function was calculated to estimate the bandwidth of the finger movement. Fig. 13(a) illustrates the impulsive force from one subject during impulsive movement. Rise times were measured to be around 30 ms for all the subjects. Fig. 13(b) plots the power spectral density function for the finger movement, and 50% bandwidth was measured to be between 5 and 7 Hz. The human finger bandwidth between 5 and 7 Hz suggests the minimum bandwidth of the thumb-controlled master–slave system should be faster than 7 Hz. As can be seen from Fig. 12(d) the bandwidth of the master–slave system is well beyond that of the human finger movement.

5. Conclusions

Robotic devices have become widely used for many surgical procedures. Current robot technology, however, has limitations to be used in MIS. Dexterous manipulation in a small space, as in the patient body, requires small actuators, yet capable of generating a sufficient number of dof. For minimally invasive procedures, ultrasonic actuators may be one of the best candidates due to their compact size and high torque characteristics at low speed.

This paper developed a new control scheme for a surgical instrument that can be used in minimally invasive surgical procedures. The surgical instrument is capable of three-dof actuation at its wrist using a single ultrasonic motor. The three-dof wrist motion of the instrument is controlled by a thumb-controlled joystick under master–slave control concept. The responsiveness of the master–slave system has been confirmed through experiments.

Intra-operative magnetic resonance imaging (MRI) is becoming a significant clinical procedure. General mechanical parts are not compatible with MR environment because of ferromagnetic materials contained in the parts. The ultrasonic actuators are not affected by the magnetic field of MRI, since they do not require coils or magnets as in electromagnetic motors [12,13].

The present study has developed a prototype of a surgical instrument that can be used in MIS. To be used in surgical environment, there are several issues to be considered, including the torque capacity and size of the multi-dof ultrasonic motor and sterilization of the instrument. While the torque capacity of the developed ultrasonic motor is high enough to generate motion in free space, it needs to be improved for contact tasks, such as suturing and knotting. The torque capacity of the USM can be improved by increasing either preload or friction coefficient between the rotor and the stator. We are currently developing a small clutch mechanism that can lock or unlock the rotor of the USM: the clutch is unlocked for free space motion, and the clutch is locked to for contact tasks to provide a higher stall torque.

Acknowledgments

This research was supported by the Japan Society of the Promotion Science. The authors gratefully acknowledge this support.

References

[1] R. Howe, Y. Matsuoka, Robotics for surgery, *Annual Reviews Biomedical Engineering* 1 (1999) 211–240.

[2] R. Bansevicius, Piezoelectric multi-degree of freedom actuators/sensors, *Proceedings of the 3rd International Conference on Motion and Vibration Control*, 1996, pp. K9–K15.

[3] T. Amano, T. Ishii, K. Nakamura, S. Uehara, An ultrasonic actuator with multi-degree of freedom using bending and longitudinal vibrations of a single stator, *Proceedings of the IEEE International Ultrasonics Symposium*, 1998, pp. 667–670.
[4] S. Toyama, S. Sugitani, G. Zhang, Y. Miyatani, K. Nakamura, Multi degree of freedom spherical ultrasonic motor, *Proceedings of the IEEE International Conference on Robotics and Automation*, 1995, pp. 2935–2940.
[5] K. Sasae, K. Ioi, Y. Ohtsuki, Y. Kurosaki, Development of a small actuator with three degrees of rotational freedom (3rd report), *Journal of the Japanese Society of Precision Engineering* 62 (4) (1996) 599–603 (in Japanese).
[6] K. Takemura, T. Maeno, Design and control of an ultrasonic motor capable of generating a multi-degrees of freedom motion, *IEEE/ASME Transactions of Mechatronics* 6 (4) (2001) 496–506.
[7] K. Takemura, T. Maeno, Method for controlling multi-DOF ultrasonic motor using neural network, *Journal of Robotics and Mechatronics* 15 (2) (2003) 534–540.
[8] S. Park, K. Takemura, T. Maeno, Study on multi-DOF ultrasonic actuator for laparoscopic instrument, *JSME International Journal, Series C: Mechanical Systems, Machine Elements and Manufacturing* 47 (2) (2004) 574–581.
[9] K. Takemura, Design of Multi-DOF USM and its Control Using Nonlinear Inverse Model, PhD Dissertation, Department of Mechanical Engineering, Keio University, Japan, 2002 (in Japanese).
[10] F. Lin, R. Wai, C. Hong, Identification and control of rotary traveling-wave type ultrasonic motor using neural networks, *IEEE Transactions on Control Systems and Technology* 9 (4) (2001) 672–680.
[11] K. Takemura, T. Maeno, Characteristics of an ultrasonic motor capable of generating a multi-degrees of freedom motion, *Proceedings of the IEEE International Conference on Robotics and Automation*, 2000, pp. 3660–3665.
[12] Y. Koseki, K. Chinzei, N. Koyachi, T. Arai, Robotic assist for MR-guided surgery using leverage and parallelepiped mechanism, *Proceedings of the International Conference on Medical Image Computing and Computer-Assisted Intervention*, 2000, pp. 940–948.
[13] D. Kim, E. Kobayashi, T. Dohi, I. Sakuma, A new, compact MR-compatible surgical manipulator for minimally invasive liver surgery, *Proceedings of the International Conference on Medical Image Computing and Computer-Assisted Intervention*, 2002, pp. 164–169.